

Resistance calculation and operational parameter optimization of an opener based on dynamic friction characteristics test of bulk materials

Renqiang Yang^{1,2}, Zhengjun Guan^{1*}, Lihua Zhang³, Yuanhang Xu¹

(1. College of Engineering and Technology, Southwest University, Chongqing 400715, China;

2. College of Smart Health, Chongqing Polytechnic University of Electronic Technology, Chongqing 401331, China;

3. School of Mechanical and Electrical Engineering, Sichuan Agricultural University, Ya'an 625014, Sichuan, China)

Abstract: Currently, friction characteristics obtained from empirical parameters or soil direct shear tests are widely applied in the resistance calculation and operational parameter optimization of soil tillage components. However, the operation of soil-touching components is a dynamic process, and there are few reports on the dynamic friction characteristics of soil-contacting components in agricultural tillage based on factors such as different moisture content, pressure, and relative velocity. Herein, a test device to measure the friction characteristics of compressible bulk materials was developed: the interface friction between the soil and 65Mn plate and the internal friction characteristics of soil were tested using this device, and the dynamic changes of interface friction coefficient and internal friction coefficient with moisture content, pressure, and relative velocity were obtained. Based on the dynamic friction parameters of soil, the ditching resistance model of a typical ploughshare opener was established, the ditching resistance value was predicted, and field experiments were performed under different operating speeds (0.5 m/s, 0.7 m/s, and 0.9 m/s) and ditching depths (60 mm, 100 mm, and 140 mm). The results indicated that the calculated values of the ditching resistance model based on the dynamic friction parameters of soil reduced the error by 15% compared with the calculated values based on the friction characteristics of the soil direct shear test, which verified the accuracy of the ditching resistance model and the validity of the parameters obtained from the test device for the friction characteristics of compressible bulk materials. In addition, the minimum ditching resistance can be obtained when the ditching speed is 0.7 m/s at the same ditching depths, which is consistent with the dynamic friction characteristics of soil. It can be found that the dynamic friction characteristics of bulk materials have basic theoretical support for the optimization of operational component structures and operational parameters.

Keywords: bulk materials, dynamic friction characteristics, ditching resistance model, operational parameter optimization

DOI: [10.25165/j.ijabe.20241706.9297](https://doi.org/10.25165/j.ijabe.20241706.9297)

Citation: Yang R Q, Guan Z J, Zhang L H, Xu Y H. Resistance calculation and operational parameter optimization of an opener based on dynamic friction characteristics test of bulk materials. *Int J Agric & Biol Eng*, 2024; 17(6): 121–130.

1 Introduction

In recent years, with the development of modern agriculture, the operational efficiency of agricultural equipment has been enhanced, and soil tillage components are the main energy consumption link during agricultural production. As the key soil-contacting component of sowing and irrigation, the opener should optimize the operational parameters, reduce its operational resistance as much as possible, and enhance the operational efficiency on the premise of ensuring operational quality^[1-4]. The technical methods for reducing the resistance of the soil-contacting components include gas or liquid filling, the vibration method, the electro-osmosis method, surface modification, and the bionic method. Most of the above methods reduce the farming resistance by changing the structural parameters of soil-contacting

components. When the structural parameters of the soil-contacting components are determined, it is of great significance to accurately predict the operational resistance and optimize the operational parameters to further reduce the operational resistance for enhancing the working efficiency^[5-9].

Currently, domestic and foreign scholars' research on the opener's operational resistance is mostly based on the empirical parameters of the opener-soil interaction and the calibration parameters obtained by discrete element simulation, thereby realizing the resistance reduction effect^[10-15]. Wang et al.^[16] established the interaction model between the soil and wing-shaped subsoiler and analyzed the influence of the wing-shaped subsoiler on soil disturbance behavior by applying discrete element method (DEM) simulation and an indoor soil tank test, which provided a reference for optimizing the wing-shaped subsoiler as a method for enhancing the soil loosening effect and reducing traction. Through theoretical calculation and kinematic analysis, Wang et al.^[17] designed a seed furrow compaction device with an opener to compact and reshape the original seed furrow, and finally formed a smooth and flat V-shaped seed furrow, which provided a reference for the design of an opener and corn precision seeder. Ahmad et al.^[18] performed discrete element simulation with EDEM software and established three-dimensional DEM models for a notched opener, toothed opener, and double-disk opener. By comparing the simulation data with the field test data, the applicability of this method under different conditions was determined. Zhang et al.^[19]

Received date: 2024-08-14 Accepted date: 2024-10-27

Biographies: Renqiang Yang, PhD candidate, research interest: agricultural material science and agricultural machinery optimization design, Email: yqr8727504@mail.swu.edu.cn; Lihua Zhang, PhD, Professor, research interest: agricultural engineering, Email: zhanglihua69@126.com; Yuanhang Xu, MS candidate, research interest: agricultural engineering, Email: xiaohangdexiang@163.com.

*Corresponding author: Zhengjun Guan, PhD, Professor, research interest: biomass energy and agricultural machinery optimization design. Southwest University, Chongqing 400715, China. Tel: +86-13351115923, Email: zhjguan@163.com.

designed a sharp-toothed opener with different structural parameters (blade thickness, blade curve, clearance angle, and front rake), and performed experiments under no-tillage conditions. The effects of different structural parameters were analyzed using the orthogonal test and single factor test. Zhang et al.^[20] summarized the biological structure of burrowing animals including beetles, crickets, and earthworms, as well as their anti-sticking and resistance-reducing mechanisms, and introduced the application of biodynamic bionic technology in Northeast China, which provided a method for developing new bionic agricultural machinery systems and meeting the conservation-tillage requirements in North China. Song et al.^[21] established the discrete element model of the opener-soil interaction and analyzed the disturbance behavior of the opener to the soil at different positions, different speeds, and different operational depths. Singh et al.^[22] analyzed the effects of different types of openers on soil impermeability, ridge height, soil disturbance, and germination rate at different operational depths and speeds, and selected the most effective openers for the establishment of sugarcane crops. Ucgul et al.^[23] constructed a discrete element model in the tillage process, which was applied to predict the soil movement, the percentage of buried surface soil, and the forward movement of soil in the process, and it was verified using a soil box. Zeng et al.^[24] designed a standard ditching blade with a self-excited vibration device and operated it in sandy clay with a 30 cm tilling depth. To perform the self-excited vibration ditching test, a simulation model of the interaction between the soil and ditching mechanism was established by coupling the ADAMS and EDEM software. Aikins et al.^[25] introduced the application of DEM in various aspects of tool-design optimization in simulating tillage and ditching. Different contact models, particle sizes and shapes, and calibration techniques utilized to determine input parameters of tillage and ditching research are expounded. Kim et al.^[26,27] applied DEM software to model the agricultural soil, simulated the traction force as a function of tilling depth, and verified the accuracy of the prediction by comparing it with the field test results.

Because soil is a compressible bulk material, its behavior is apparently inconsistent with the assumption of discrete element simulation; it is, therefore, difficult to realize the accurate prediction of operational resistance. Currently, most design parameters applied in openers are obtained using the soil-direct shear test or soil-accumulation angle test, which is apparently different from the actual operational condition. However, the operation of soil-touching components is a dynamic process characterized by a change of speed, and there are few reports on the dynamic friction characteristics of compressible bulk materials such as soil and livestock manure based on pressure, relative velocity, and moisture content. Therefore, it is necessary to explore the dynamic friction characteristics between the soil and soil-touching components and the dynamic internal friction characteristics of soil as a method of optimizing the opener's structural parameters and operational parameters.

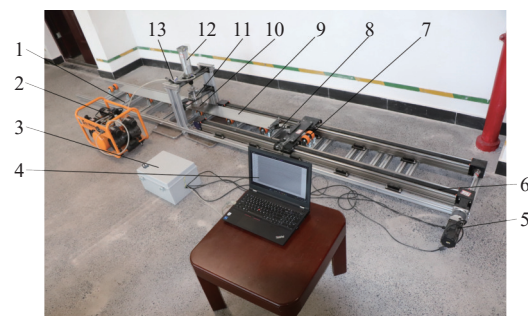
Therefore, this study developed a test device to measure the friction characteristics of compressible bulk materials to reveal the dynamic friction characteristics of the interface between the soil and operational components and the dynamic internal friction characteristics of soil. Based on the obtained friction characteristics parameters, the ditching resistance was predicted by establishing a ditching resistance calculation model. Additionally, the correctness of the ditching resistance model and the effectiveness of the dynamic friction characteristics parameters were verified using field

experiments, which provided basic theoretical support for the research and development of soil-contacting components and the optimization of operational parameters.

2 Materials and methods

2.1 Test device

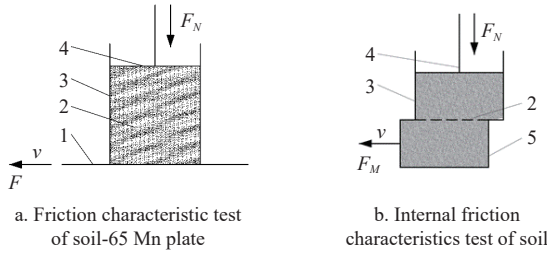
To obtain the dynamic friction characteristics of the interface between the soil and different material plates and the dynamic internal friction parameters of soil, a test device to measure the friction characteristics of compressible bulk materials was developed. As depicted in Figure 1, the test device comprises a mechanical system, a control system, and a test system. The mechanical system comprises the following: underframe, pulley, slide rail assembly mechanism, test plate, fixed cylinder, and moving cylinder. Among them, the test plate is a plate of different materials, and the test plate of 65Mn steel is used in this study. The control system controls the servo-motor parameters, such as rotational speed, relative motion speed, and cylinder pressure. Cylinder pressure is used to control the vertical pressure of the bulk material. The test system accurately measures and stores parameters such as relative motion speed, cylinder pressure, and the synchronous belt tension. By changing the charging cylinder's installation mode, the test device can test the dynamic friction characteristic parameters between the soil and plate interface and the dynamic internal friction characteristic parameters that characterize soil.



1. Underframe 2. Air compressor 3. Control box 4. Test system 5. Servo motor 6. Slide rail assembly 7. Pulley 8. Tension sensor 9. Test plate 10. Moving cylinder 11. Fixed cylinder 12. Air cylinder 13. Pneumatic control valve

Figure 1 Test device for dynamic friction characteristics of compressible bulk materials

The test principle is shown in Figure 2. During the dynamic friction characteristic test between the soil and plate interface, as shown in Figure 2a, soil with certain moisture content is loaded into the cylinder 3, a certain pressure value is set for the cylinder, and the cylinder applies constant pressure to the material in the cylinder through the pressure plate. Thus, the soil in the cylinder is in close contact with the plate, the stress is uniform, and the servo motor is set with different rotating speeds through the control system to drive the synchronous belt and the test plate 1 to move horizontally at a uniform speed. Therefore, the test plate and the soil generate dynamic friction. When the tension F is in a stable state, the moving speed of the plate is detected by the speed sensor, and the plate's transverse pulling force is detected by the pulling force sensor. According to the cylinder pressure, the plate's pulling force and the relative moving speed, the variation law between the maximum static friction coefficient of soil and the plate, the interface friction coefficient and the relative moving speed, the soil moisture content, and the positive pressure can be obtained.



1. Steel plate of 65Mn 2. Soil 3. Fixed cylinder 4. Pressure plate 5. Moving cylinder

Figure 2 Test principle of dynamic friction characteristics

As shown in Figure 2b, for soil shear, when the dynamic internal friction characteristic test is performed, the fixed cylinder 3 is raised, the moving cylinder 5 is installed below it, and cylinder 3 is ensured to be coaxial with cylinder 5. When the cylinder is filled, different pressures and speeds are set, the cylinder piston drives the plate to press the material downwards, and the servo motor drives the moving cylinder through the synchronous belt to perform the dynamic internal friction characteristic test of the materials.

2.2 Test materials

The experimental soil was sandy cohesive soil in the southwest mountainous area of China, which was obtained from an agricultural experimental field in Jiulongpo District, Chongqing. The test soil was naturally air-dried, placed on a rubber board, and ground with wood to fully disperse the soil structure. Meanwhile, impurities such as large-particle plant roots and gravel were removed, the ground soil sample was put into a 110°C oven to dry, the sample was bagged and sealed at room temperature to cool, and test soil samples with 10%, 20%, and 30% moisture contents were prepared, each with 1 kg. The thickness, width, and surface roughness of the 65Mn plate are 2 mm, 110 mm, and 6.3 μm, respectively.

2.3 Test method

2.3.1 Interface dynamic friction test between the soil and the 65Mn plate

As illustrated in Figure 2a, when the soil in the fixed cylinder is filled, the pressure plate exerts a certain downward-acting pressure on the soil, and the motor pulls the 65Mn plate through the synchronous belt to conduct the tests for the interface friction characteristics. By setting different vertical pressure, soil moisture content, and relative motion speed, the corresponding interface friction coefficient can be obtained, and the calculation formula is as follows:

$$\mu_1 = \frac{F - F_0}{F_N} \quad (1)$$

where, μ_1 denotes the interface friction coefficient; F denotes the friction resistance of the plate; F_0 denotes the frictional resistance at no load; and F_N denotes the vertical pressure.

To obtain the dynamic friction characteristics between the soil and 65Mn plate interface, the tests were conducted comprehensively, with a total of 75 groups of tests, and each group of experiments was repeated 3 times, as illustrated in Table 1.

2.3.2 Dynamic internal friction test of soil

As depicted in Figure 2b, the corresponding internal friction coefficient of soil can be obtained by different vertical pressure, soil moisture content, and relative motion speed, and the calculation formula is as follows:

$$\mu_2 = \frac{F_M - F_0}{F_N} \quad (2)$$

where, μ_2 denotes the internal friction coefficient; F_M denotes internal friction resistance, N.

To obtain the law regulating the dynamic internal friction characteristics of soil, the tests were conducted comprehensively, with a total of 75 groups of tests, and each group of tests was repeated three times, as listed in Table 2.

Table 1 Comprehensive test scheme for dynamic friction characteristics between the soil and 65Mn plate interface

| Moisture content/% | Pressure/N | Velocity/m·s ⁻¹ |
|--------------------|------------|----------------------------|
| 10 | 400 | 0.1 |
| 20 | 800 | 0.3 |
| | 1200 | 0.5 |
| 30 | 1600 | 0.7 |
| | 2000 | 0.9 |

Table 2 Comprehensive test scheme for dynamic internal friction characteristics of soil

| Moisture content/% | Pressure/N | Velocity/m·s ⁻¹ |
|--------------------|------------|----------------------------|
| 10 | 400 | 0.1 |
| 15 | 800 | 0.3 |
| | 1200 | 0.5 |
| 20 | 1600 | 0.7 |
| | 2000 | 0.9 |

2.3.3 Soil direct shear test

In the test, a ZJ strain-controlled direct shear apparatus produced by Nanjing Soil Instrument Company was utilized. As depicted in Figure 3, the soil was prepared into circular cutter samples under the following moisture contents: 10%, 20%, and 30%. The sample size exhibited a 61.8 mm diameter and 20 mm height, and the controlled dry density was 1.5 g/cm³. The vertical pressures of each group of tests during shearing were 125 kPa, 250 kPa, 375 kPa, and 500 kPa. The shear rate was 0.8mm/min, and the theoretical formula of the soil direct shear test is the Coulomb equation^[28].

$$\tau_{\max} = c + p \tan \varphi \quad (3)$$

where, τ_{\max} denotes the maximum shear stress, Pa; c denotes soil cohesion; p denotes the vertical pressure, Pa; and φ denotes the internal friction angle of soil, (°).



Figure 3 Soil direct shear test

3 Test results and data analysis

3.1 Analysis of dynamic friction characteristics between the soil and 65Mn plate interface

As illustrated in Figure 4, the interface friction coefficient of soils with different moisture contents changed with pressure. From

Figure 4a, it can be observed that the interface friction coefficient between soils with 10% moisture content and the 65Mn plate first increased and subsequently decreased with the increase in pressure. When the relative velocities were 0.1 m/s, 0.3 m/s, 0.7 m/s, and 0.9 m/s, the interface friction coefficient peaked at a 1.2 kN pressure value, and subsequently began to decrease. For the soil with a 10% moisture content, before the water film appeared on the interface (i.e., when the pressure was less than 1.2 kN), the soil–interface contact area gradually increased with the increase in

pressure, which led to an increase in the interface friction coefficient. When the pressure exceeded 1.2 kN, the water film effect first appeared at the interface, and then became more apparent with the increase in pressure.

It can be observed from Figure 4b that the interface friction coefficient of soil with a 20% moisture content had an apparent downward trend with the increase in pressure: the water film effect formed between the soil and interface was more apparent with the increase in positive pressure.

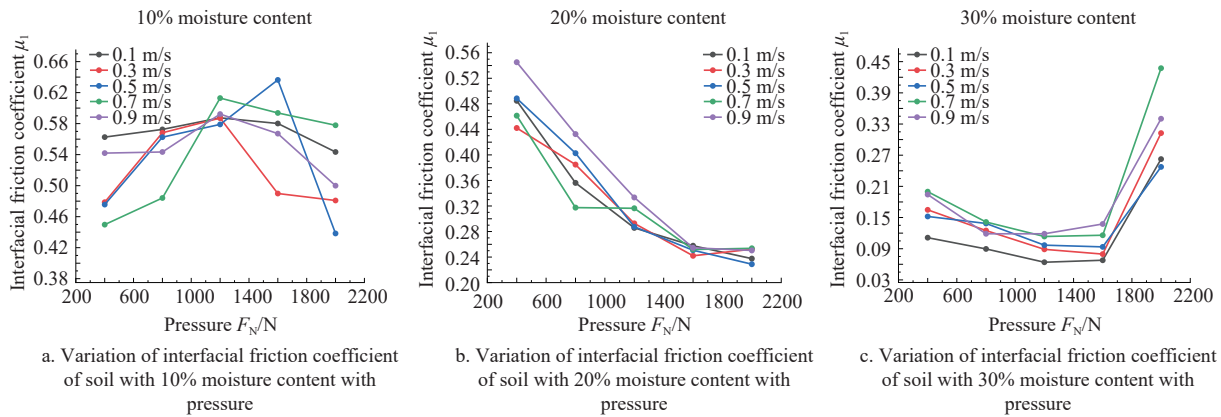


Figure 4 Variation of interface friction coefficient between the soil and 65Mn plate with pressure

It can be noted from Figure 4c that the interface friction coefficient of soil with a 30% moisture content first decreased and subsequently increased with the increase in pressure. When the pressure was less than 1.6 kN, there was an apparent trend of gradual decline with the increase in pressure, and the minimum value appeared at the 1.6 kN pressure value, which can be explained as follows: when the pressure exceeded 1.6 kN, the water film between the soil and the interface was destroyed, leading to a sharp increase in the interface friction coefficient.

As illustrated in Figure 5, the interface friction coefficient of soils with different moisture contents changed with the relative velocity. From Figure 5a, it can be observed that the interface

friction coefficient of soils with 10% moisture content first decreased and subsequently increased with the increase in relative velocity. When the pressure value attained 400 N and 800 N, the minimum interface friction coefficient was obtained when the relative velocity was 0.7 m/s; when the pressure value was 1.2 kN and 2 kN, the minimum interface friction coefficient was obtained when the relative velocity was 0.5 m/s; and when the pressure value was 1.6 kN, the minimum interface friction coefficient was obtained when the relative velocity was 0.3 m/s. At low moisture content, the seepage velocity of water was affected by soil density, and the formation speed of the interface water film was closely related to the relative movement speed.

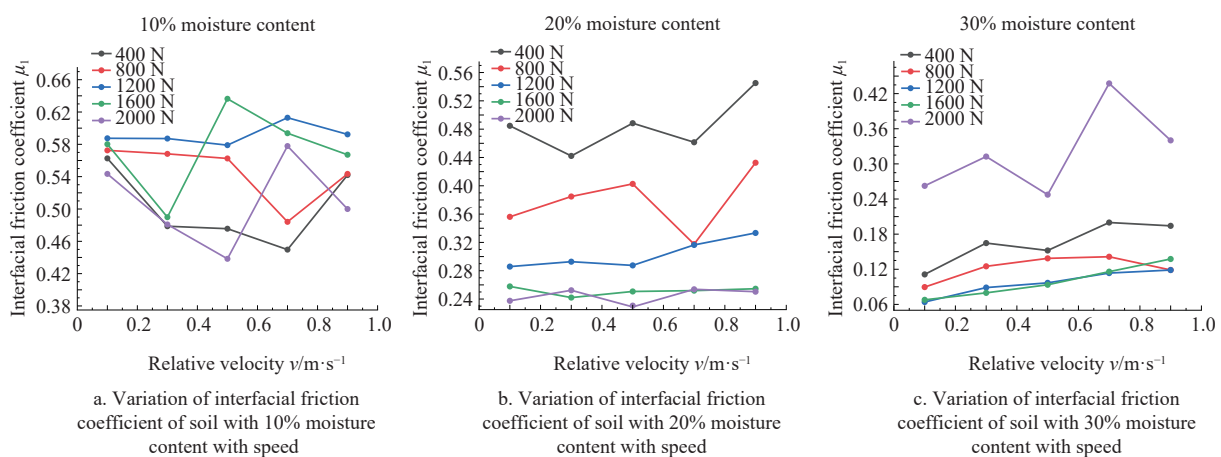


Figure 5 Variation of friction coefficient between the soil and 65Mn plate interface with speed

It can be noted from Figure 5b that the interface friction coefficient of soil with a 20% moisture content increased slowly with the increase of relative velocity, and a trough appears at the relative velocity of 0.7 m/s when the pressures were 400 N and 800 N. In addition, the lower the pressure, the greater the interface friction coefficient, which can be rationalized as follows: the soil with 20% moisture content formed a more optimal water film effect under a

slightly higher pressure.

It can be observed from Figure 5c that the interface friction coefficient of soil with 30% moisture content increased slowly with the increase of relative velocity, and the smaller the pressure, the greater the friction coefficient. However, under the 2 kN test pressure, the friction coefficient was larger and had the minimum value at the 0.5 m/s relative velocity, which is attributable to the

accelerated water loss of soil with high moisture content under high pressure, leading to a large friction coefficient.

3.2 Analyzing dynamic internal friction characteristics of soil

In the dynamic internal friction test of soil, by measuring the internal friction of soil under different vertical pressures, the soil cohesion and internal friction angle are calculated according to the Coulomb equation, and the results are listed in Table 3.

Table 3 Shear strength index of the dynamic internal friction test of soil

| Moisture content/% | Relative velocity/m·s ⁻¹ | Apparent cohesion/kPa | Internal friction angle/(°) |
|--------------------|-------------------------------------|-----------------------|-----------------------------|
| 10 | 0.5 | 23.58 | 15.27 |
| 20 | 0.7 | 15.97 | 16.71 |
| 30 | 0.9 | 20.19 | 17.70 |

As illustrated in Figure 6, the internal friction coefficient of soils with different moisture content changed with pressure. From

Figures 6a and 6c, it can be noted that the internal friction coefficient of soils with 10% and 20% moisture contents gradually decreased with the increase in pressure, and the higher the moisture content, the more apparent the trend, which can be explained as follows: with the increase in pressure, the more water seeps out of the soil particles, the more apparent the water film effect inside the soil. It can be noted from Figure 6b that the internal friction coefficient of soil with 15% moisture content gradually decreased with the increase in pressure when the relative velocity was 0.7 m/s and 0.9 m/s. When the relative velocity was 0.1 m/s, 0.3 m/s, and 0.5 m/s, the internal friction coefficient of the soil with 15% moisture content first decreased and subsequently increased with the increase in pressure. Additionally, the internal friction coefficient attained the minimum value at the 1.2 kN pressure value, and subsequently started to increase, which indicates that the water film effect of the soil with 15% moisture content began to undergo gradual destruction when the pressure exceeded 1.2 kN.

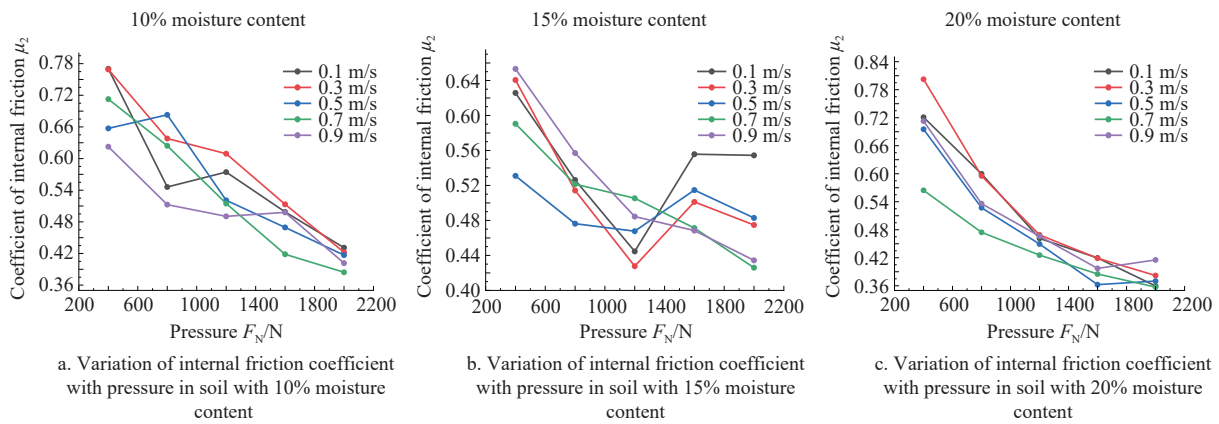


Figure 6 Variation of internal friction coefficient in soil with pressure

As depicted in Figure 7, the internal friction coefficient of soils with different moisture contents changed with the relative velocity. From Figure 7a, it can be noted that the internal friction coefficient of soil with 10% moisture content first increased and subsequently decreased with the increase in relative velocity when the pressure

was 800 N, and it had the maximum internal friction coefficient when the relative velocity was 0.5 m/s. At other pressures, the internal friction coefficient decreased with the increase in relative velocity.

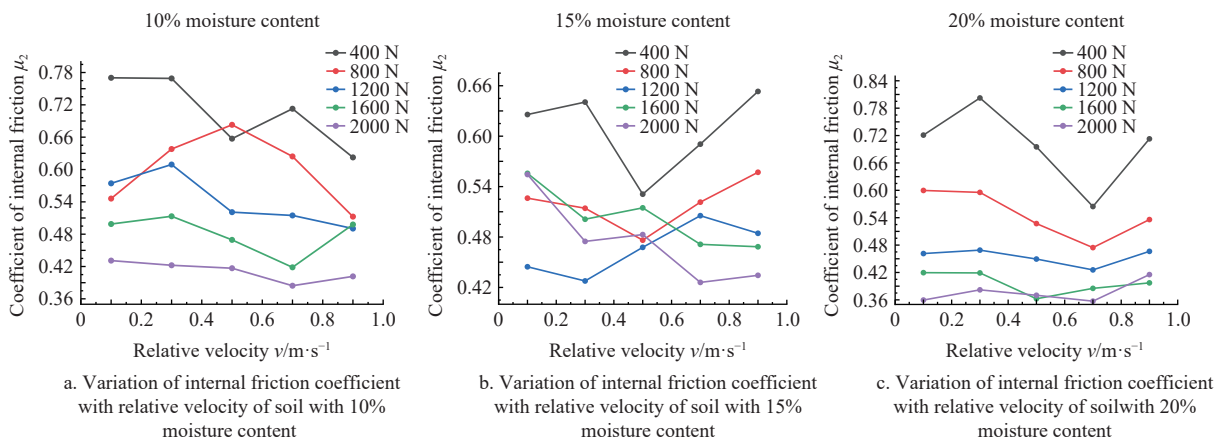


Figure 7 Variation of internal friction coefficient of soil with relative velocity

As illustrated in Figure 7b, when the pressure was 400 N, 800 N, and 1.2 kN, the internal friction coefficient of soil with 15% moisture content first decreased and subsequently increased with the increase in relative velocity. The minimum internal friction coefficient at 400 N and 800 N appeared at the relative velocity of 0.5 m/s, and the minimum internal friction coefficient at 1.2 N

appeared at the relative velocity of 0.3 m/s. When the pressure was 1.6 kN and 2 kN, the internal friction coefficient of soil with 15% moisture content decreased gradually with the increase in relative velocity.

It can be noted from Figure 7c that the internal friction coefficient of soil with 20% moisture content first decreased and

subsequently increased with the increase in relative velocity, and the minimum internal friction coefficient mostly appeared at the relative velocity of 0.7 m/s. In addition, the greater the pressure, the smaller the internal friction coefficient.

3.3 Soil direct shear test results

In the soil direct shear test, by measuring the soil shear force under different vertical pressures, the soil cohesion and internal friction angle are calculated according to Coulomb's formula. The results are listed in Table 4.

Table 4 Shear strength index of the soil direct shear test

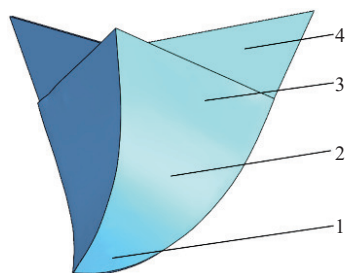
| Moisture content/% | Apparent cohesion/kPa | Internal friction angle/(°) |
|--------------------|-----------------------|-----------------------------|
| 10 | 35.73 | 23.75 |
| 20 | 17.9 | 20.3 |
| 30 | 10.01 | 11.86 |

The internal friction angle obtained in this test is only related to moisture content and pressure, and does not consider the influence of the motion velocity of soil particles on the internal friction angle. Therefore, the cohesion force and internal friction angle obtained in this test are different from the parameters obtained in the above dynamic friction characteristic test.

4 Mechanical model analysis of ditching resistance

4.1 Force analysis of the opener

The operational quality and ditching resistance of the ploughshare opener have a direct influence on the plow surface, and the design of the plow surface is related to the guide curve and the element line angle. According to the principle of the horizontal straight-line method stipulated in agricultural mechanics, the plow surface is a continuous plow surface that is formed by the parallel movement of the straight element line along the guide curve as per the angle θ of the element line. The structure of the opener is depicted in Figure 8, including the soil-lifting surface and soil-guiding surface, the turning surface, and the side blade.



1. Soil-lifting surface 2. Soil-guiding surface 3. Turning surface 4. Side blade
Figure 8 Structure diagram of opener

When the opener is working, it can generally be regarded as a uniform linear motion in the soil. Meanwhile, its force is in a state of equilibrium, the soil's force on it is a pair of interactive forces, and the force is equal. Therefore, only the horizontal component of the force between the opener and the soil is required to determine its required ditching resistance.

When the opener is working, it is necessary to provide cutting force F_q and inertial force F_g to lift the soil and friction force f between the surface and the soil at every moment. The horizontal component equations of these three forces can be obtained as per the following principle: the opener is in equilibrium when working, the force is synthesized and decomposed, as illustrated in Formula 4, and the tillage resistance F_d of the ploughshare opener can subsequently be obtained.

$$F_d = F_{qx} + f_x + F_{gx} \tag{4}$$

where, F_d denotes the opener's tillage resistance, N; F_{qx} denotes the horizontal component of the cutting force, N; f_x denotes the horizontal component of the friction force, N; and F_{gx} denotes the horizontal component of the inertial force, N.

When the opener is working, the soil block is formed in front of it. The shape of the soil block comprises the working surface of the opener, the ground surface, and the end and side surfaces of the soil block, as illustrated in Figure 9. The height of the soil block is consistent with the opener's tilling depth h , the angle between the side of the soil block and the direction of operation is the internal friction angle ϕ , and the angle between the front end surface and the opener's vertical direction is also ϕ .

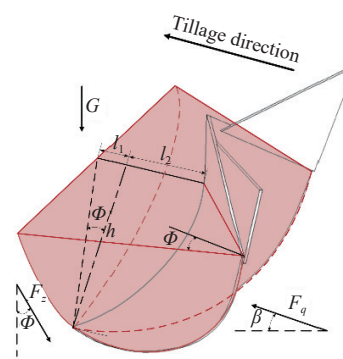


Figure 9 Shape and parameters of soil block

4.2 Cutting force analysis of the opener

Divide the soil block into two symmetrical soil blocks based on the opener's cutting line, as depicted in Figure 9. For each soil block, the sample is subjected to its own gravity G , soil shear resistance F_z , and cutting force F_q in the ditching process. When the soil is cut, it can be determined that the force of the soil block satisfies the following equation:

$$\begin{cases} F_{qx} = 2F_q \cos\beta = 2F_z \sin\phi \\ F_z = (F_q \sin(\frac{\pi}{2} - \beta - \phi) + G \sin\phi) \tan\phi + C \cdot S \\ G = \rho g V \end{cases} \tag{5}$$

where, ρ is the soil's density, g/cm^3 ; g denotes the acceleration of gravity, 9.8 m/s^2 ; V denotes the volume of a single soil block, mm^3 ; ϕ denotes the internal friction angle, ($^\circ$); C denotes the cohesion of the soil, kPa; S denotes the shear area between soils, m^2 ; and β denotes the angle between cutting force and horizontal plane, ($^\circ$).

4.3 Friction force analysis of the opener

During the working process of the opener, the plow surface makes contact with the soil, and relative motion occurs, thereby generating friction between the plow surface and soil. To facilitate the analysis and construction of the model, the friction force acting on the opener is analyzed, as illustrated in Figure 10. The friction force tangents the plow surface and has a certain angle with the opener's moving direction; therefore, the friction force acting on the plow surface can be calculated by the following equation:

$$\begin{cases} f_x = 2f_{1x} + 2f_{2x} \\ f_{1x} = f_1 \cdot \cos\alpha \cdot \cos\varphi_1 \\ f_{2x} = f_2 \cdot \cos\beta_2 \cdot \cos\varphi_1 \\ f_1 = \mu_3(G_1 \cdot \cos\alpha \cdot \sin\varphi_2 + F_{N1} \cdot \sin\alpha \cdot \sin\varphi_2) \\ f_2 = \mu_4(G_2 \cdot \cos\beta_2 \cdot \sin\varphi_3 + F_{N2} \cdot \sin\beta_2 \cdot \sin\varphi_3) \end{cases} \tag{6}$$

where, f_{1x} denotes the horizontal component of the friction force on

the tip of the trencher, N; f_{2x} denotes the horizontal component of the friction force on its waist surface, N; f_1 denotes the friction force on its tip, N; f_2 denotes the friction force on its waist surface, N; α denotes the penetration angle, ($^\circ$); β_2 denotes the angle between the friction force on the waist surface and the horizontal plane, ($^\circ$); φ_1 denotes the angle between the horizontal component of the friction force and the direction of operation, ($^\circ$); φ_2 denotes the angle between the approximate plane of the tip component and the central vertical plane where the cutting line is located, ($^\circ$); φ_3 denotes the angle between the micro plane of the waist surface and the central vertical plane where the cutting line is located, ($^\circ$); θ denotes the angle of the elementary line corresponding to the depth of the ploughing height, ($^\circ$); μ_3 denotes the interface friction coefficient of the tip component; μ_4 denotes the friction coefficient of the waist surface component; G_1 denotes the soil weight of the tip component, N; G_2 denotes the soil weight of the waist curved component, N; F_{N_1} denotes the soil extrusion pressure of the tip component, N; F_{N_2} denotes the soil extrusion pressure of the waist curved component, N; and N_f denotes the normal supporting force of the soil block, N.

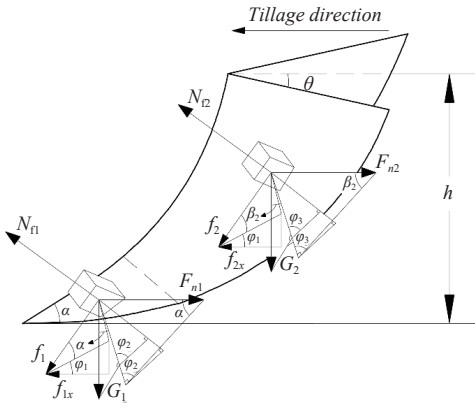


Figure 10 Friction calculation diagram of soil block

4.4 Inertial force analysis of the opener

When the plowshare opener operates optimally, the soil blocks in front gradually rise under the action of the opener, indicating that the opener should provide additional inertial force to lift the soil blocks, which can be calculated by impulse and momentum theorem. As illustrated in Figure 11, there is a closed control body in front of the opener, whose volume and shape are consistent with soil blocks. Because the opener keeps moving at a constant speed when working, soil blocks flow out of the control body, and new wedge-shaped soil blocks enter the control body; therefore, the inertial force F_{gx} can be calculated by the following formula:

$$\begin{cases} F_{gx} = F_g \sin \phi = \frac{dm}{dt} v \sin \phi \\ v = \frac{dh}{\cos \phi dt} = \frac{v_0}{\sin \phi} \\ \frac{dm}{dt} = \rho \cdot S_A \cdot \frac{dh}{dt} = \rho \cdot S_A \cdot \frac{v_0}{\tan \phi} \end{cases} \quad (7)$$

where, F_{gx} denotes the horizontal component of the inertial force, N; F_g denotes the inertial force, N; dm denotes the mass of soil flowing out of the control body per unit time, kg; v denotes the speed of the soil block relative to the bottom of the control body, m/s; dh denotes the height of the soil block gushing out of the control body, m; v_0 denotes the opener's operation speed, m/s; ρ denotes the density of the soil block, g/cm³; and S_A denotes the area of the control body's upper surface, mm².

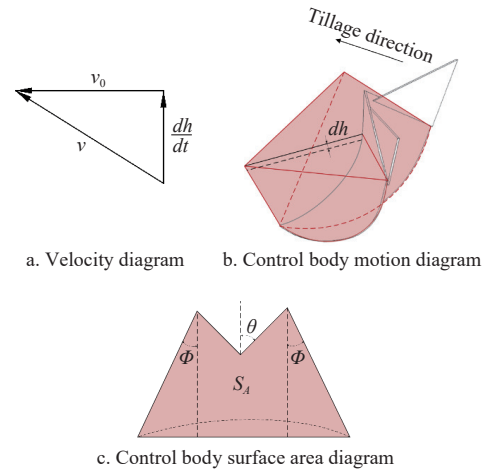


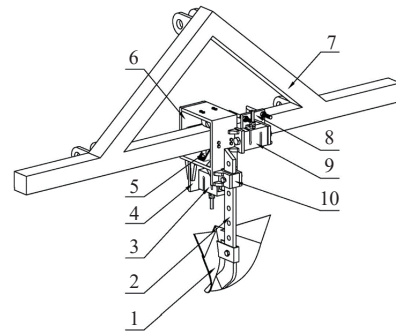
Figure 11 Schematic diagram of inertial force calculation

5 Field ditching experiment

To further verify the law regulating the dynamic friction characteristics of soil and the accuracy of the ditching resistance model based on the dynamic friction characteristics, a field ditching experiment was conducted considering the effects of ditching depth, working speed, and soil moisture content.

5.1 Test device

As depicted in Figure 12, the developed field ditching resistance test device is driven using an agricultural tractor. The resistance test device for field ditching operation comprises a traction tripod, a test frame, a measuring system, and an opener component. The test frame includes a main frame, rollers, a frame cover, a fixing plate, and an opener mounting frame. The measuring system comprises a mobile power supply, a longitudinal force sensor, a transverse force sensor, a data acquisition module, and data processing and analysis software. The opener component includes an opener and an opener mounting handle. The resistance test device of the field ditching operation is driven by an agricultural tractor. After the opener cuts into the soil, the longitudinal ditching resistance and lateral resistance of the opener during the operation can be obtained by the longitudinal force sensor and the lateral force sensor, respectively.



1. Opener 2. Opener mounting handle 3. Longitudinal force sensor 4. Main frame 5. Roller 6. Frame cover 7. Traction tripod 8. Fixing plate 9. Transverse force sensor 10. Opener mounting frame

Figure 12 Resistance test device for field ditching operation

The structural parameters of the experimental opener are listed in Table 5, the opener's guide curve equation is illustrated in Equation (8), and its straight-line angle fitting equation is depicted in Equation (9).

The parameter equation of the guide curve of the opener is

expressed as

$$f(x) = \begin{cases} 0.47x, & (0 < x \leq 27.19) \\ 0.03x^2 - 2.09x + 54.61, & (27.19 < x \leq 93.01) \\ 17.83x, & (93.02 < x \leq 96.3) \end{cases} \quad (8)$$

Table 5 Structural parameters of the opener

| Height of leading curve h/mm | Lifting angle $\varepsilon/(\circ)$ | Angularity of tangent line $\omega/(\circ)$ | Opening of the leading curve L/mm | Minimum element angle $\theta_{\min}/(\circ)$ | Maximum element angle $\theta_{\max}/(\circ)$ |
|---------------------------------------|-------------------------------------|---|--|---|---|
| 185 | 25 | 118 | 96.3 | 40 | 58 |

The angle fitting equation of the straight element line of the opener is expressed as

$$\begin{cases} \theta = \theta_{\min} + my_i \\ y_i = \frac{6.2x^2}{x^2 + 100} \\ m = \frac{\theta_{\max} - \theta_{\min}}{y_{\max}} \end{cases} \quad (9)$$

where, θ denotes the angle of the straight element line, (\circ); θ_{\min} denotes the minimal angle of the straight element line, (\circ); θ_{\max} denotes the maximum angle of the straight element line, (\circ); m denotes the proportionality coefficient; x, y are the moving point coordinates of the X - Y coordinate system with θ_{\min} as the origin.

5.2 Test conditions

The test site is an agricultural field in Jiulongpo District, Chongqing, with a plot measuring 10 m long and 1 m wide. The agricultural tractor used in the test is a Dongfeng-404 wheel tractor. Before the experiment, the soil was rotary tilled once with a rotary tiller, and the soil was leveled. Subsequently, the physical properties of the soil were measured, including bulk density and moisture content. The results are listed in Table 6.

Table 6 Parameters of the physical properties of soil in the test plot

| Parameter | Depth/mm | Average value |
|---|----------|---------------|
| Density/($\text{g}\cdot\text{cm}^{-3}$) | 0-140 | 1.55 |
| Moisture content/% | 0-140 | 20.1 |

5.3 Test plan

As depicted in Figure 13, because the opener's structure is symmetrical with two wings, the lateral operational resistance in the ditching process is ignored, and only the longitudinal ditching resistance should be detected. The opener was comprehensively tested at three operational speeds and three ditching depths, with 9 groups. After each operation, the soil was leveled and the position of the opener was adjusted, with a 10 m distance for each test. Each group of tests was repeated 3 times, and the specific test groups are listed in Table 7.

5.4 Analysis of test results

By substituting the structural parameters, dynamic friction coefficient, and parameters in Tables 3 and 4 into Equations (5)-(9), the cutting force, friction force, and inertial force are obtained respectively, and then the values of the above three forces are substituted into Equation (4) to obtain the ditching resistance based on dynamic friction characteristic parameters and the ditching resistance based on direct shear test friction characteristic parameters, as shown in Figure 14.

Figure 14 is a comparative diagram of longitudinal ditching resistance obtained from the field ditching test and ditching

resistance calculated from the mechanical model. Figure 14a is the ditching resistance calculated by the mechanical model based on the dynamic friction characteristic parameters of soil, and Figure 14b is the ditching resistance calculated by the mechanical model based on the friction characteristic parameters of the soil direct shear test.



Figure 13 Field ditching test

Table 7 Field ditching test grouping

| Test number | Tillage speed/ $\text{m}\cdot\text{s}^{-1}$ | Ditching depth/mm |
|-------------|---|-------------------|
| 1 | 0.5 | 60 |
| 2 | 0.5 | 100 |
| 3 | 0.5 | 140 |
| 4 | 0.7 | 60 |
| 5 | 0.7 | 100 |
| 6 | 0.7 | 140 |
| 7 | 0.9 | 60 |
| 8 | 0.9 | 100 |
| 9 | 0.9 | 140 |

Figure 14 indicates that the tilling depth greatly influenced the ditching resistance: the greater the tilling depth, the greater the ditching resistance. At the same tilling depth, the ditching resistance in the field test first decreased and subsequently increased with the increase in operational speed, and had the minimum ditching resistance at the 0.7 m/s operational speed.

As illustrated in Figure 14a, for the field test and the ditching resistance calculated based on the dynamic friction characteristic parameters, the minimum ditching resistance was obtained at the 0.7 m/s operating speed under different ditching depths, which is consistent with the dynamic friction characteristic law of soil. When the ditching depth was 60 cm, the average deviation between the calculated value and the measured value obtained by field experiment of ditching resistance was 6.4%; when the ditching depth was 100 cm, the average deviation between the two resistance values was 7.9%; when the ditching depth was 140 cm, the average error between the two resistance values was 8.8%. The error value increased with the increase in ditching depth, which can be explained as follows: under constant working speed, with the increase in ditching depth, the ditching resistance calculation model fills the surface of the opener with soil for hypothetical calculation. However, in the ditching field test, the surface of the opener within the ditching depth was not completely covered with soil due to the irregular distribution of soil in the experimental plot, which led to a scenario where the error between the calculated value and the test value gradually increased with the increase in ditching depth.

As depicted in Figure 14b, the calculated ditching resistance based on the parameters of soil friction characteristics in the direct shear test kept increasing with the increase in operational speed at

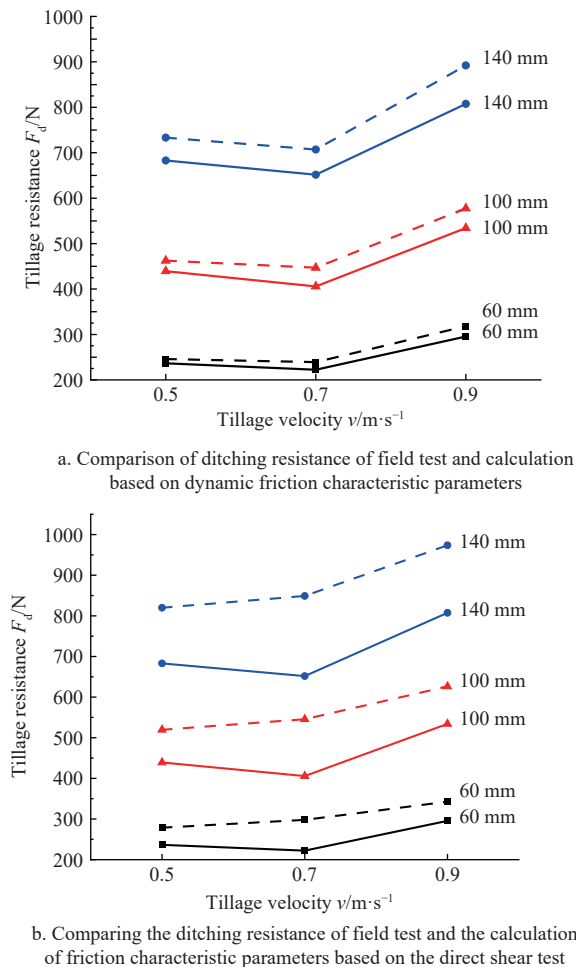


Figure 14 Comparing the ditching resistance calculated by the field test and mechanical model (Solid line represents field test value, and dashed line represents calculated value)

the same tilling depth, which is inconsistent with the dynamic friction characteristics of soil and the change law of ditching resistance in the field test. When the ditching depth was 60 cm, the average deviation between the calculated value and the measured value obtained by field experiment of ditching resistance was 21.3%; when the ditching depth was 100 cm, the average deviation between the two resistance values was 23.3%; when the ditching depth was 140 cm, the average error between the two resistance values was 23.6%.

It can be observed that the error between the ditching resistance value and the test value calculated based on the dynamic friction characteristic parameters was smaller than that calculated by the friction characteristic coefficient of the soil direct shear test, and the error value was reduced by 15%.

This observation indicates that the ditching resistance calculated based on dynamic friction characteristic parameters is more consistent with the actual working state than that calculated based on traditional test methods.

6 Conclusions

(1) The formation of a water film on the interface is the main influencing factor for the dynamic friction coefficient, and the relative movement speed of the soil and interface, positive pressure, and soil moisture content significantly affect the state of the water film. With the increase in pressure, the interface friction coefficient between the soil with 10% moisture content and the 65Mn plate first

increases and subsequently decreases, whereas the interface friction coefficient between the soil with 20% moisture content and 30% moisture content slowly increases with the increase in relative velocity.

(2) The water seepage from soil particles significantly affects the water-film effect in soil. The internal friction coefficient of soil with a 10% and 20% moisture content decreases gradually with the increase in pressure, and the minimum internal friction coefficient of soil with a 20% moisture content appears when the relative velocity is 0.7 m/s. Additionally, the tilling depth greatly influences the ditching resistance, and the greater the tilling depth, the greater the ditching resistance. At the same tilling depth, the overall trend of ditching resistance increases with the increase in operational speed, and the opener exhibits the minimum ditching resistance at the 0.7 m/s speed, which is consistent with the dynamic friction characteristics of soil.

(3) Based on the dynamic friction characteristics of bulk materials, the operational resistance and optimal operational parameters of soil-contacting components, material extrusion, conveying components, and material mixing components in agricultural farming can be calculated and predicted more accurately, and the structural parameters of operational components can be optimized more accurately. Thus, the energy consumption can be further decreased.

Acknowledgements

This work was financially supported by China Agriculture Research System (Grant No. CARS-02) and Chongqing Science and Technology Bureau Agricultural High Tech Special Project (Grant No. CSTC2019ngzx0017).

[References]

- [1] Wang L J, Zhou B, Wan C, Zhou L. Structural parameter optimization of a furrow opener based on EDEM software. *Int J Agric & Biol Eng*, 2024; 17(3): 115–120.
- [2] Pöhlitz J, Rücknagel J, Koblenz B, et al. Computed tomography and soil physical measurements of compaction behaviour under strip tillage, mulch tillage and no tillage. *Soil and Tillage Research*, 2018; 175: 205–216.
- [3] Sadiq M, Li G, Rahim N, Tahir M M. Sustainable conservation tillage technique for improving soil health by enhancing soil physicochemical quality indicators under wheat mono-cropping system conditions. *Sustainability*, 2021; 13(15): 8177.
- [4] Aikins K A, Barr J B, Antille D L, Ucgul M, Jensen T A, Desbiolles J M A. Analysis of effect of bentleg opener geometry on performance in cohesive soil using the discrete element method. *Biosystems Engineering*, 2021; 209: 106–124.
- [5] Barr J B, Ucgul M, Desbiolles J M A, Fielke J M. Simulating the effect of rake angle on narrow opener performance with the discrete element method. *Biosystems Engineering*, 2018; 171: 1–15.
- [6] Tekeste M Z, Balvanz L R, Hatfield J L, Ghorbani S. Discrete element modeling of cultivator sweep-to soil interaction: Worn and hardened edges effects on soil-tool forces and soil flow. *Journal of Terramechanics*, 2019; 82: 1–11.
- [7] Zeng Z W, Chen Y. Performance evaluation of fluted coulters and rippled discs for vertical tillage. *Soil & Tillage Research*, 2018; 183: 93–99.
- [8] Barr J B, Desbiolles J M A, Fielke J M, Ucgul M. Development and field evaluation of a high-speed no-till seeding system. *Soil and Tillage Research*, 2019; 194: 104337.
- [9] Aikins K A, Jensen T A, Antille D L, Barr J B, Desbiolles J M A. Evaluation of bentleg and straight narrow point openers in cohesive soil. *Soil and Tillage Research*, 2021; 211: 105004.
- [10] Zeng Z W, Chen Y, Zhang X R. Modelling the interaction of a deep tillage tool with heterogeneous soil. *Computers and Electronics in Agriculture*, 2017; 143: 130–138.
- [11] Qin K, Ding W M, Ahmad F, Fang Z C. Design and experimental validation of sliding knife notch-type disc opener for a no-till combine

- harvester cum seed drill. *Int J Agric & Biol Eng*, 2018; 11(4): 96–103.
- [12] He C, You Y, Wang D, Wang G, Lu D, John M T K. The effect of tine geometry during vertical movement on soil penetration resistance using finite element analysis. *Computers and Electronics in Agriculture*, 2016; 130: 97–108.
- [13] Ma C, Qi J T, Kan Z, Chen S J, Meng H W. Operation power consumption and verification tests of a trenching device for orchards in Xinjiang based on discrete element. *Int J Agric & Biol Eng*, 2021; 14(1): 133–141.
- [14] Liu G M, Yao J Y, Chen Z, Han X K, Zou M. Mesoscopic analysis of drag reduction performance of bionic furrow opener based on the discrete element method. *Plos one*, 2023; 18(11): e0293750.
- [15] Liu D J, Gong Y, Zhang X J, Yu Q X, Zhang X, Chen X, et al. EDEM simulation study on the performance of a mechanized ditching device for codonopsis planting. *Agriculture*, 2022; 12(8): 1238.
- [16] Wang X Z, Li P, He J P, Wei W Q, Huang Y X. Discrete element simulations and experiments of soil-winged subsoiler interaction. *Int J Agric & Biol Eng*, 2021; 14(1): 50–62.
- [17] Wang W J, Diao P S, Jia H L, Chen Y L. Design and experiment evaluation of furrow compaction device with opener for maize. *Int J Agric & Biol Eng*, 2020; 13(2): 123–131.
- [18] Ahmad F, Qiu B J, Ding Q S, Ding W M, Khan Z M, Shoaib M, et al. Discrete element method simulation of disc type furrow openers in paddy soil. *Int J Agric & Biol Eng*, 2020; 13(4): 103–110.
- [19] Zhang X C, Li H W, Du R C, Ma S C, He J, Wang Q J, et al. Effects of key design parameters of tine furrow opener on soil seedbed properties. *Int J Agric & Biol Eng*, 2016; 9(3): 67–80.
- [20] Zhang Z J, Jia H L, Sun J Y. Review on application of biomimetic for designing soil-engaging tillage implements in Northeast China. *Int J Agric & Biol Eng*, 2016; 9(4): 12–21.
- [21] Song C Y, Zhang X C, Li H, Lv Y C, Li Y G, Wang X L, et al. Effect of tine furrow opener on soil movement laws using the discrete element method and soil bin study. *Inmatch-Agricultural Engineering*, 2022; 68: 350–366.
- [22] Singh S, Tripathi A, Singh A K. Effect of Furrow opener design, furrow depth, operating speed on soil characteristics, draft and germination of sugarcane. *Sugar Tech*, 2017; 19: 476–484.
- [23] Ucgul M, Saunders C, Fielke J M. Discrete element modelling of tillage forces and soil movement of a one-third scale mouldboard plough. *Biosystems Engineering*, 2017; 155: 44–54.
- [24] Zeng Y, Li H C, Li J, Zhang Q Q, Li C, Li Z, et al. Research on the ditching resistance reduction of self-excited vibrations ditching device based on MBD-DEM coupling simulation. *Frontiers in Plant Science*, 2024; 15: 1372585.
- [25] Aikins K A, Ucgul M, Barr J B, Awuah E, Antille D L, Jensen T A, et al. Review of discrete element method simulations of soil tillage and furrow opening. *Agriculture*, 2023; 13: 541.
- [26] Kim Y S, Siddique M A A, Kim W S, Kim Y J, Lim R G. DEM simulation for draft force prediction of moldboard plow according to the tillage depth in cohesive soil. *Computers and Electronics in Agriculture*, 2021; 189: 106368.
- [27] Kim Y-S, Lee S-D, Baek S-M, Baek S-Y, Jeon H-H, Lee J-H, et al. Development of DEM-MBD coupling model for draft force prediction of agricultural tractor with plowing depth. *Computers and Electronics in Agriculture*, 2022; 202: 107405.
- [28] Briend R, Radziszewski P, Pasini D. Virtual soil calibration for wheel-soil interaction simulations using the discrete-element method. *Canadian Aeronautics & Amp Space Journal*, 2011; 57(1): 59–64.